ELSEVIER

Journal of Electron Spectroscopy and Related Phenomena 86 (1997) 25–40

JOURNAL OF ELECTRON SPECTROSCOPY and Related Phenomena

Collected works of Theo Thole: the spectroscopy papers

Frank de Groot[a,*], Gerrit van der Laan[b]

[a]*University of Groningen, Nijenborgh 4, 9747 AG Groningen, Netherlands*
[b]*Daresbury Laboratory, Warrington WA4 4AD, UK*

Abstract

The work of the late Theo Thole is introduced in five sections, discussing (1) multiplet theory, (2) the branching ratio, (3) dichroism and sum rules, (4) X-ray photoemission and (5) resonant X-ray scattering. At the end of the paper a complete list of all papers published by Theo Thole is included. © 1997 Elsevier Science B.V.

Keywords: Multiplet theory; X-ray magnetic dichroism; X-ray absorption; Sum rules; X-ray scattering; Photoemission; Branching ratio; Auger; Charge-transfer; Impurity model

1. Introduction

This article is written to serve as a first introduction to the papers published by Theo Thole. The reference list contains all articles on which Theo has participated ([1–94]). It is strongly recommended that the reader studies the original papers, which contain all the mathematical details and numerous beautiful observations on core spectroscopy by Theo and his co-authors. In this article only Theo's papers on core level spectroscopy are discussed. This implies that his early work ([1–14]) is not included. For a discussion of this early work the reader is referred to the articles by Piet van Duijnen and Jan Kommandeur in this issue. Over the last 10 years Theo Thole developed a computer program which is able to describe all core level spectroscopies of strongly correlated systems, within the single-impurity Anderson model. Historically, the theory was developed first with the description of X-ray absorption spectra, as will be outlined in Section 2.

2. Multiplet theory of X-ray absorption

This section sketches the historical development of the description of X-ray absorption spectra of rare earths and transition metals. This "multiplet theory of X-ray absorption" has been developed by Theo Thole, in collaboration with Gerrit van der Laan and the groups of Professors Akio Kotani, Takeo Jo and George Sawatzky. In the description below the historical order is followed, introducing step-by-step atomic multiplet theory, crystal-field multiplet theory and charge-transfer multiplet theory.

2.1. Atomic multiplet theory

Atomic multiplet theory has been developed to explain atomic spectra. One of the successful atomic multiplet programs has been developed by Cowan. In 1985 Theo used this Cowan program to describe the X-ray absorption spectra of manganese in a solid. The paper entitled 'New probe for the ground state electronic structure of narrow band and impurity states' [15] demonstrated the potential of X-ray absorption of the solid state. Dipole transitions from the ground

* Corresponding author.

PII S0368-2048(97)00046-7

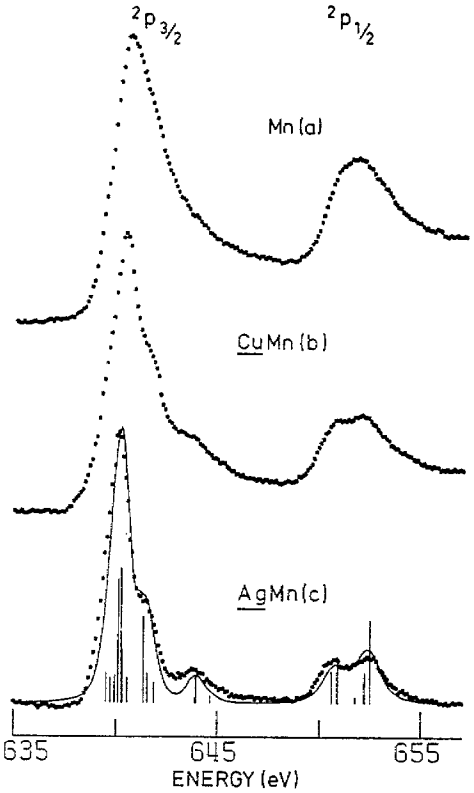

Fig. 1. The Mn 2p X-ray absorption (EELS) spectra of: (a) pure Mn metal; (b) 3.5% Mn in Cu; (c) 5% Mn in Cu. (Reproduced with permission from Ref. [15]. Copyright 1985 American Physical Society.)

state can reach only a limited subset of final states, thereby providing a fingerprint for the specific ground state. Using the atomic multiplet program it was shown that dilute manganese in silver unambiguously displays the atomic Hund rule $3d^5$ ground state [$^6S_{5/2}$]. By comparison with experiment all other ground state symmetries could be ruled out. Fig. 1 (reproduced from [15]) compares the 2p X-ray absorption spectral shape to the atomic multiplet theory.

The atomic multiplet Hamiltonian can be written as:

$$H_{\text{atom}} = \tfrac{1}{2}\sum_{\nu_1,\nu_2,\nu_3,\nu_4} g_{\nu\nu}(\nu_1,\nu_2,\nu_3,\nu_4)a^\dagger_{\nu_1}a^\dagger_{\nu_2}a_{\nu_3}a_{\nu_4} + \sum_{\nu_1,\nu_2,c_1,c_2} g_{\nu c}(\nu_1,c_1,c_2,\nu_2)a^\dagger_{\nu_1}a^\dagger_{c_1}a_{c_2}a_{\nu_2} + \sum_{\nu_1,\nu_2}\xi(\nu_1,\nu_2)a^\dagger_{\nu_1}a_{\nu_2} + \sum_{c_1,c_2}\xi(c_1,c_2)a^\dagger_{c_1}a_{c_2} \quad (1)$$

Here, ν and c are the valence states and the core states respectively. ξ is the spin–orbit interaction, $g_{\nu\nu}$ the multipole Coulomb interaction between the valence states and $g_{\nu c}$ the multipole Coulomb and exchange interaction between valence and core states.

Using the atomic multiplet model, 3d adsorption of all rare earths were calculated and compared to measured high-resolution X-ray absorption spectra [17]. The comparison of the multiplet calculations for the Hund rule ground states with the calculations for all multiplet states confirms the presence of the Hund rule ground state and the importance of the dipole selection rules. Different valences of a given rare earth show different line shapes and are displaced in energy, opening up the way to mixed valence studies on, for instance, Ce and Tb. Theo discovered that the line shapes only matched when a strong saturation in the photo-yield signal was assumed, being due to the short absorption length of the order of tens of an angstrom. This length scale was later confirmed within good accuracy by experimental studies [27].

2.2. Crystal field multiplet theory

Over the next 10 years Theo extended Cowan's multiplet program to crystal field symmetry by including the code of Phil Butler, allowing calculations in any point group. The first results appeared in 'Spin-mixed ground state of Fe phthalocyanine' [23], where a choice of two different ground states was offered to match with the experimental data. It was proposed to use the temperature dependence of the branching ratio to determine the precise nature of the ground state. In 'Multiplet structure in the $L_{2,3}$ X-ray absorption spectra' [29] it was demonstrated how the spectra of compounds with different spin could be clearly distinguished.

The additional term in the Hamiltonian due to the crystal field strength can be indicated as:

$$H_{\text{crystalfield}} = \sum_{\nu_1,\nu_2} D_{\nu_{1,2}}a^\dagger_{\nu_1}a_{\nu_2} \quad (2)$$

Here $D_{\nu_{1,2}}$ is the electrostatic field coupling the atomic representations within the point group symmetry of the system. Systematic studies of compounds in octahedral symmetry, yielding excellent agreement with experimental results, were presented in 'X-ray absorption edges of d_0 compounds' [37]. It

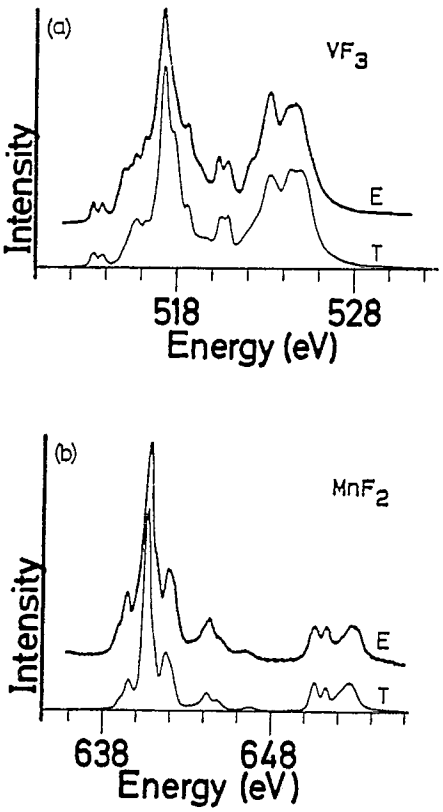

Fig. 2. The 2p X-ray absorption spectra (E) of (a) VF_3 and (b) MnF_2 compared with crystal field multiplet calculations (T). (Reproduced with permission from Ref. [38]. Copyright 1990 American Physical Society.)

was shown that the splitting between the two main peaks in both the L_3 and L_2 edges is related, though not equal, to the crystal-field splitting.

In '2p X-ray absorption of 3d transition-metal compounds' [38] an overview is given of the spectral shapes in octahedral symmetry. Fig. 2 (reproduced from [38]) compares the 2p X-ray absorption spectral shape to the crystal field multiplet theory. Comparison with high-resolution 2p X-ray absorption spectra shows excellent agreement, which confirmed the validity of the approach. In general, ionic compounds can be described in great detail. An important application of this approach is to determine the valence, spin-state, point-group symmetry and crystal-field strength of transition metal ions in complex systems. This approach has been applied to the symmetry of Ca atoms at the surface of CaF_2 and at the CaF_2/Si interface [50].

2.3. Charge transfer multiplet theory

Another essential extension of the multiplet program was the introduction of configuration interaction or, in other words, the single-impurity Anderson model. The importance of the impurity Anderson model for correlated systems had been well established, and the combination to a single model of the multiplet model and the impurity Anderson model was a very important step in the understanding of core level spectroscopy. The Hamiltonian of the single-impurity Anderson model can be written as:

$$H_{\mathrm{IAM}} = \sum_{k,\nu} \epsilon_k a^\dagger_{k\nu} a_{k\nu} + \epsilon_\nu \sum_\nu a^\dagger_\nu a_\nu + \epsilon_c \sum_c a^\dagger_c a_c + \frac{V}{\sqrt{N}} \sum_{k,\nu} (a^\dagger_\nu a_{k\nu} + a^\dagger_{k\nu} a_\nu) + U_{\nu\nu} \sum_{\nu>\nu'} a^\dagger_\nu a_\nu a^\dagger_{\nu'} a_{\nu'} - U_{\nu c} \sum_{\nu,c} a^\dagger_\nu a_\nu (1 - a^\dagger_c a_c) \quad (3)$$

Here, the summations over ν and c represent the summation over the spin and orbital quantum numbers. The ligand band (ϵ_k), the valence level (ϵ_ν) and the core level (ϵ_c) interact with each other via the valence level—ligand band hybridization (V), the Coulomb interaction between valence electrons ($U_{\nu\nu}$) and the core-hole potential ($U_{\nu\nu}$)

The Anderson impurity model was used in 'Theory of multiplet structure in 4d core photoabsorption spectra of CeO_2' [35]. With the Anderson impurity model it is possible to incorporate solid state effects of the hybridization between 4f and valence band. In 'Theory of X-ray absorption spectra in PrO_2 and some other rare earth compounds' [48] and 'Praseodymium 3d and 4d core photoemission spectra of Pr_2O_3' [47] it was shown that the interplay between the atomic multiplet coupling and the solid-state hybridization between rare-earth 4f and oxygen 2p states is essential in determining the spectral shapes of 3d-XPS, 4d-XPS and 4d-XAS.

The Anderson impurity model, or charge-transfer multiplet model, has been applied to transition metal compounds in 'Evidence of local singlet state in $NaCuO_2$ from copper 2p X-ray photoemission and absorption spectra' [51]. In 'Charge transfer satellites and multiplet splitting in X-ray photoemission spectra of late transition metal halides' [58] the core-level X-ray photoemission spectra (XPS) are calculated for a cluster model. Intra-atomic multiplet coupling as

well as covalency mixing is taken into account. The overall spectral shape of the Ni 2p XPS can be explained by a charge transfer mechanism, and the difference in the line shape between the Ni $2p_{3/2}$ and $2p_{1/2}$ XPS spectra is shown to originate from the multiplet splitting of their charge transfer satellites.

The contribution of Kotani and Ogasawara in this issue reviews the use of the charge transfer multiplet model applied to rare earths.

3. The branching ratio

The 2p branching ratio is the ratio between the L_3 edge and the L_2 edge in X-ray absorption. It is formally defined as the intensity of the L_3 edge, normalized by the total intensity: $L_3/(L_3 + L_2)$. A crucial experimental factor is the possibility to determine the branching ratio with simple X-ray absorption experiments whereby high resolution of the experiment is not necessary. In a series of papers the predictive power of the branching ratio has been outlined.

Preceding the branching ratio series, the paper 'Identification of the relative population of spin–orbit split states in the ground state of a solid' [20] showed that it was possible to investigate experimentally the relative populations of the $4f_{7/2}$ and $4f_{5/2}$ spin–orbit split states in the ground state of Ce, not only by looking at the detailed fine structure but also by studying the relative intensity ratio of the $3d_{5/2}$ and $3d_{3/2}$ absorption structures. The first hunch came in the theoretical study 'Systematics of the relation between spin–orbit splitting in the valence band and the branching ratio in X-ray absorption spectra' [21]. The behaviour of the branching ratio was related to spin–orbit coupling in the ground state. However, regarding this behaviour the paper mentioned "we could not find a proof nor a physical explanation, but we verified it empirically for the p → d transitions in transition metal atoms and the d → f transitions in rare earth metal atoms".

Only one year later this proof was found. In the paper 'Linear relation between X-ray absorption branching ratio and valence-band spin–orbit expectation value' [25] the first angular momentum diagrams appeared. Fig. 3, reproduced from [25], shows the application of the YLV4 theorem in order to simplify the momentum coupling in the calculation of the

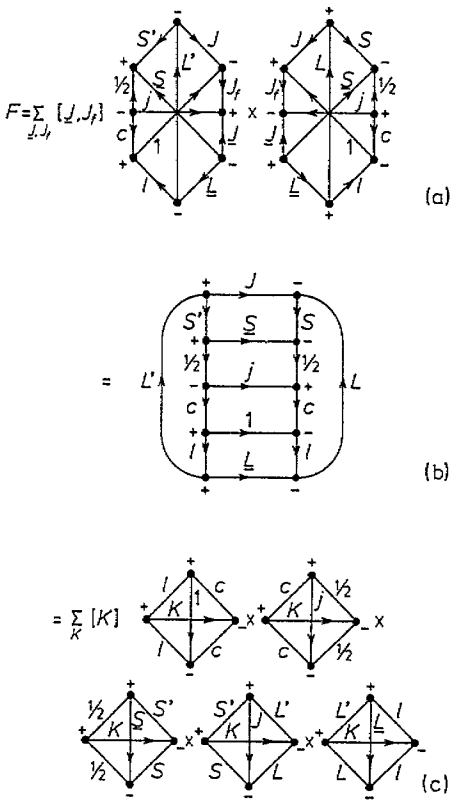

Fig. 3. The evaluation of the term F, which is used in the dipole matrix element P_j. (Reproduced with permission from Ref. [25]. Copyright 1988 American Physical Society.)

dipole matrix element P_j. With the use of this theorem it was mathematically demonstrated that the branching ratio is proportional to the expectation value of the angular-dependent part of the spin–orbit interaction. For a p → d transition:

$$B = \frac{2}{3} - \frac{1}{3\langle n_h \rangle} \left\langle \sum_i l_i \cdot s_i \right\rangle \tag{4}$$

Together with the proportionality of the total signal to the number of holes in the ground state, the result for the branching ratio gives the sum rule for the isotropic spectrum. In 'Local probe for spin–orbit interaction' [28] and 'Branching ratio in X-ray absorption spectroscopy' [24] the origins of nonstatistical branching ratios in spin–orbit-split X-ray absorption spectra were explained. Atomic calculations for transition metals show a systematic change which is due to initial-state spin–orbit splitting and electrostatic interactions between core hole and valence electrons. This

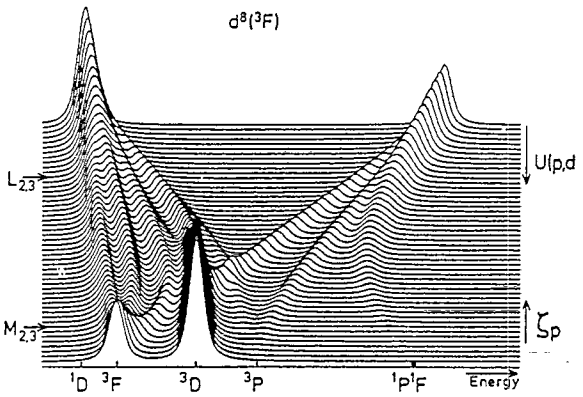

Fig. 4. The calculated transition probability of the transition $3d^8 \rightarrow 2p^5 3d^9$ for the ^3F initial state. (Reproduced with permission from Ref. [24]. Copyright 1988 American Physical Society.)

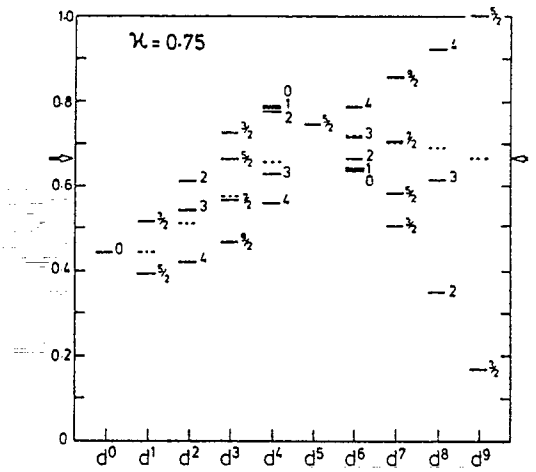

Fig. 5. Calculated branching rations for the indicated J levels of the Hund rule ground state in the transition $3d^n \rightarrow 2p^5 3d^{n+1}$, using U_{pd} scaled to 75% of their Hartree-Fock calculated values. (Reproduced with permission from Ref. [24]. Copyright 1988 American Physical Society.)

resulted in general rules, which are also applicable to solids. The first rule states:

Rule 1. In the absence of both spin–orbit coupling in the initial state and electrostatic interactions between core hole and valence electrons in the final state the branching ratio is statistical.

A direct interpretation of the spin state of experimental spectra is possible using the second rule:

Rule 2. High-spin states have on average a larger branching ratio than low-spin states,...

In the free atom the branching ratio reaches a maximum for the high-spin (Hund rule) ground state and its value decreases gradually for S, L and J levels of higher energy. The use of either LS-coupling or jj-coupling is nicely illustrated in Fig. 4. The top spectrum has zero 2p3d interactions (U_{pd}), hence a statistical branching ratio, and it identifies with jj-coupling. The bottom spectrum has zero core spin–orbit splitting (ζ_p) and identifies with LS-coupling. The arrows on the left side of Fig. 4 indicate the approximate situations of U_{pd}/ζ_p for the 2p and 3p core states.

The situation for the branching ratio for the 2p edges in the 3d transition metals was found to be complex. First, U_{pd}/ζ_p is approximately unity, implying intermediate coupling. Second, the 3d spin–orbit coupling is not negligible, and the combined effects are indicated in Fig. 5.

A further complication is the presence of a crystal field, which results in a lower branching ratio when it produces a low-spin ground state. Another potential effect of crystal fields is a quenching of the 3d spin–orbit coupling. The rules and figures in [24,28] can be used to assess the spin state and the spin–orbit splitting from the experimental branching ratio in transition metals and rare earths.

A first attempt to explain the branching ratio of dichroism spectra can be found in 'Magnetic dichroism in the X-ray absorption branching ratio' [36]. In this paper it is explained that the branching ratio of a core-hole-to-valence-band dipole spectrum of a magnetically ordered metal compound can have a strong polarization dependence. This circular and linear dichroism of the branching ratio can be used to assess the local magnetic structure of transition metal and rare earth compounds when no details of the multiplet structure can be observed. This paper can be viewed as a predecessor of the sum rules as developed for magnetic circular dichroism.

4. Magnetic X-ray dichroism (MXD)

In 'Strong magnetic dichroism predicted in the $M_{4,5}$ X-ray absorption spectra of magnetic rare earth materials' [16] a theory was presented predicting an anomalously large magnetic X-ray dichroism effect. Since the linear dichroism is sensitive to $\langle M^2 \rangle$ it can be used for ferromagnetic as well as antiferromagnetic materials. Interesting in this paper is the use of the

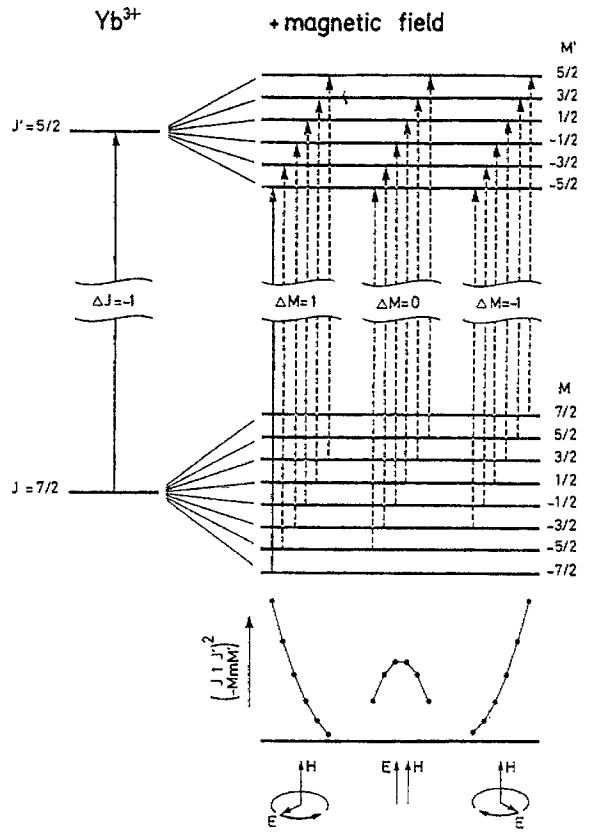

Fig. 6. Diagram of the $4f^{13} \rightarrow 3d^9 4f^{14}$ transition in Yb^{3+}. At 0 K only the transition indicated with the solid line is allowed. (Reproduced with permission from Ref. [30]. Copyright 1988 American Physical Society.)

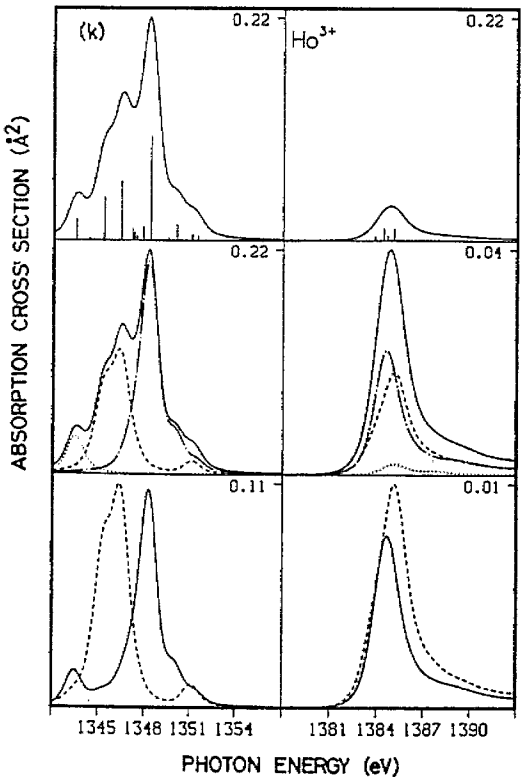

Fig. 7. Results of the multiplet calculations for the $^5I_8$ Hund rule ground state of Ho^{3+} ($4f^{10} \rightarrow 3d^9 4f^{11}$). On the left the M_5 edge, on the right the M_4. From top to bottom, the X-ray absorption spectral shape, the division into $\Delta J = -1$ (– · –), $\Delta J = 0$ (– – –) and $\Delta J = +1$ (· · ·). The bottom spectra are the spectra parallel (– – –) and perpendicular (————) to the magnetic field. (Reproduced with permission from Ref. [30]. Copyright 1988 American Physical Society.)

statistical operators in the form of Boltzmann weighted 3*j* symbols. This theoretical prediction was in 1986 quickly followed by an 'Experimental proof of magnetic X-ray dichroism' [18] on Tb 3d in Tb–Fe-garnet, which actually has not the most simple magnetic structure to analyze, but showed a clear and large effect.

A systematic study of all rare earths was presented in 'Calculations of magnetic X-ray dichroism in the 3d absorption spectra of the rare earths' [30]. Fig. 6 is a pictorial figure of the MXD in Yb^{3+}, which can be found in many review articles. With the aid of this figure one is able to understand most effects of circular and linear dichroism. The $^2F_{7/2}$ ground state of Yb^{3+} is split by a magnetic field into its M_J levels. At zero temperature only $\Delta M_J = -1$ transitions can occur. On increasing the temperature the excited states also get populated and $\Delta M_J = 0$ and $\Delta M_J = +1$ become possible. Magnetic circular dichroism (MCD) is given as $(\Delta M_J = -1) - (\Delta M_J = +1)$ and linear dichroism (MLD) is given as $(\Delta M_J = -1) + (\Delta M_J = +1) - 2(\Delta M_j = 0)$. Because the X-ray absorption intensities are proportional to the 3*j*-symbol,

$$\begin{pmatrix} J & 1 & J' \\ -M_J & \Delta M_J & M'_J \end{pmatrix}^2 \tag{5}$$

which implies that for large values of J, both the MCD and the MLD closely follow the ΔJ transition. This was visualized in [30] for all rare earths and Fig. 7 gives the example of holmium (with $J = 8$). One can observe that the linear dichroism (bottom) follows very closely the different sets of ΔJ

transitions (middle), which gives rise to very pronounced MLD, as well as MCD, effects. During the last 10 years it became clear that the linear dichroism effects in rare earth systems are often dominated by crystal field effects. A method to produce circularly polarized X-ray was proposed in [31], but as is the case of many good theoretical ideas, the device was never put into practice.

Calculations of MCD at the $L_{2,3}$ edges of Gd metal, which take into account dipole transitions to the spin-polarized conduction bands as well as quadrupole transitions to the highly localized 4f states were presented in 'Magnetic X-ray dichroism in gadolinium metal' [46]. The quadrupolar dichroism is important in determining the pre-edge structure of the measured spectra. Whether these quadrupole transitions in the MXD spectrum were really of practical importance remained a topic for debate after their theoretical prediction until, in 1995, convincing evidence was produced in favour of their existence from the angular and temperature dependence. The contribution of van Veenendaal, Goedkoop and Thole in the present issue discusses the "breathing effects" of the 5d orbitals and its consequences for the interpretation of the $L_{2,3}$ MCD [91].

In 'Strong magnetic X-ray dichroism in 2p absorption spectra of 3d transition metal ions' [44] it was shown that the spectral shape changes drastically with the character of the ground state, which is determined by the presence of a crystal field, and the relative magnitudes of the exchange and 3d spin–orbit interaction. It was also shown that the difference in integrated intensity of the 2p absorption for left- and right-circular polarization provides a measure for the 3d spin–orbit coupling in spherical and crystal-field symmetry. The anisotropic branching ratio depends on the spin–orbit interaction and the Van Vleck contribution of the exchange interaction. Atomic calculations of the magnetic dichroism in 4d and 5d X-ray absorption spectra of trivalent actinide ions were presented in 'Calculation of magnetic X-ray dichroism in 4d and 5d absorption spectra of actinides' [49].

A new effect on the X-ray absorption line shape was described in 'Magnetic X-ray dichroism study of the nearest neighbour spin–spin correlation function' [81]. In this paper it was shown that the double-peaked L_2 edge in NiO films grown on (100) MgO is dependent on (a) the temperature and (b) the angle Θ between the polarization direction and [100]. One finding was that also at the magic angle ($3\cos^2\Theta = 1$) there is a temperature dependence. These findings could all be explained by including the effects of an exchange field. The exchange field of about 0.1 eV is able to shift the intensity within the L_2 edge. It was described how to use this effect to study the nearest neighbour spin–spin correlation function, the Neél temperature, the exchange parameter J and the local magnetic moment [81].

4.1. Sum rules

The paper of Theo which has become most famous is his *Physical Review* letter describing a new magneto-optical sum rule for X-MCD in 'X-ray circular dichroism as a probe of orbital magnetization' [52]. It was shown that the integral of the X-MCD signal over a given edge allows one to determine the ground state expectation value of the orbital magnetic moment L_z. This was a very important step for X-MCD, because the integrated intensity of the signal could be related to a ground state expectation value. In 'X-ray circular dichroism and local magnetic fields' [65] further sum rules were derived for the circular dichroic response of a core line. They relate the intensity of the X-MCD signal to the ground state expectation value of the magnetic operators (L_z, S_z and T_z) of the valence electrons. Sum rules for linear dichroism and sum rules for quadrupolar transitions were presented in 'Magnetic X-ray dichroism' [66].

Sum rules were derived for magnetic dichroism in spin-polarized photoemission from partly filled shells which give the expectation values of the orbital and spin magnetic moments and their correlations in the ground state. In 'Sum rules for magnetic dichroism in rare earth 4f photoemission' [62] this was applied to the 4f photoemission of rare earths, where the polarization effects are two orders of magnitude larger than in 3d transition metals.

Theo was always very eager to condense general knowledge into simple rules. After deriving the sum rules he took a keen interest in spectral moment analysis. Integrated intensities as supplied by sum rules correspond to the zeroth moment of the spectral distributions. The spectral shape contains additional information in the form of higher moments which can be related to ground state properties multiplied

by final state parameters. In 'Magnetic ground-state properties and spectral distributions' [72,73] a method of statistical moments for polarized spectra was developed. The potential of the method was shown by a rederivation of the X-ray absorption sum rules and branching ratio rules for the isotropic spectrum and linear and circular dichroism. Sum rule-type results were derived to obtain orbital and spin magnetic moments from polarized core level photoemission. The spin and orbital moments were obtained from the first statistical moment of the spin spectrum and the circular dichroism.

In 'X-ray absorption sum rules in *jj*-coupled operators and ground state moments of actinide ions' [85] sum rules for magnetic X-ray dichroism, relating the signals of the spin–orbit split core level absorption edges to the ground state spin and orbital operators, were expressed in *jj*-coupled operators. These sum rules can be used in the region of intermediate coupling by taking into account the cross-term between the ground state levels and are, therefore, particularly useful in the study of actinides.

4.2. The Thole sum rules

In memory of Theo the sum rules used in the field of X-ray spectroscopies should be named Thole sum rules. As stated above, in papers [43,52,62,65,66,71–73] the MCD sum rules were derived, and later unified. The result was that from the combination of X-ray absorption, its linear and circular dichroism, and spin-polarized photoemission, it is possible to determine all simple tensors, hence all moments.

Following essentially the 'Origin of spin polarization and magnetic dichroism in core level photoemission' [43], the sum rules will be introduced for the transition $c \rightarrow l$ using proportionality constants c_n which depend only on the values of c and l. For all details and proofs the reader is referred to the original papers. The integrated sum over the complete edge can be indicated with the $\mathcal{T}^{00}$ Thole sum rule. The first number refers to the orbital moment, in other words it refers to the X-ray polarization P defined as $P = 1$ for circular dichroism (left minus right polarization) and $P = 2$ for linear dichroism (left plus right minus two times z polarization). The second number refers to the spin moment, i.e. to the spin of the electron P_S, where $P_S = 0$ is spin-summed and $P_S = 1$ is the spin-difference. The orbital moment ($M = 1$) can be deduced from circular polarized X-rays ($\mathcal{T}^{10}$) and the quadrupole moment ($M = 2$) can be found from linear polarized X-rays ($\mathcal{T}^{20}$). These are the three Thole sum rules for X-ray absorption. In the next section the three further sum rules for spin-polarized photoemission will be discussed.

The $\mathcal{T}^{00}$ sum rule applies to unpolarized X-ray excitations. It determines the number of holes $\langle n_h \rangle$ in the bands to which the core electron is excited:

$$\langle n_h \rangle = c_0 \int_{edge} (\sigma_L + \sigma_R + \sigma_Z) \tag{6}$$

This sum rule is also known as the initial state rule, relating the intensities of XAS spectra to the initial state, in contrast to the energy positions (spectral shapes) which are given with the final state rule and correspond to the higher spectral moments derived in [72,73]. The $\mathcal{T}^{10}$ sum rule for circular dichroism determines the orbital moment:

$$\langle L_z \rangle = c_1 \int_{edge} (\sigma_L - \sigma_R) \tag{7}$$

The orbital moment is related to the integrated difference between left and right circular polarized X-rays. Note that this sum rule assumes the determination of the absolute X-ray absorption cross-sections, which then can be directly related to the orbital moment. The $\mathcal{T}^{20}$ sum rule for linear dichroism determines the quadrupole moment:

$$\langle Q_{zz} \rangle = c_2 \int_{edge} (2\sigma_Z - \sigma_L - \sigma_R) \tag{8}$$

The quadrupole moment, or in other words the quadrupole charge distribution, is given by the integrated difference between grazing and normal incident X-rays. Again this sum rule is exact for absolute cross-sections. The problem of the unknown absolute X-ray absorption cross sections can be overcome by dividing the $\mathcal{T}^{10}$ orbital moment and $\mathcal{T}^{20}$ quadrupole moment sum rules by the overall absorption cross-section $\mathcal{T}^{00}$. A direct way to determine the spin-expectation value of the 3d electrons is by spin-polarized photo-emission. The integrated difference between spin-up and spin-down electrons emitted from the valence band is a direct measure of the spin-moment $\langle S_z \rangle$, given by the $\mathcal{T}^{01}$ sum rule:

$$\langle S_z \rangle = 2c_0 \int (\sigma_+) - (\sigma_-) \tag{9}$$

Table 1
Calculation of the six fundamental spectra from the six basic combinations of orbital moment (+ 1, − 1,0) and spin (↑ , ↓). The sum rules are given for respectively 2p-XAS, 2p-XPS and 3d-XPS of a 3d transition metal oxide

	μ_+	μ_-	μ_0	$\int_{2p}$-XAS	$\int_{2p}$-XPS	$\int_{3d}$-XPS	$\mu_+^\uparrow$	$\mu_-^\uparrow$	$\mu_0^\uparrow$	$\mu_+^\downarrow$	$\mu_-^\downarrow$	$\mu_0^\downarrow$
I^{00}	+ 1	+ 1	+ 1	$\langle n_h \rangle$	I	$\langle n_h \rangle$	+ 1	+ 1	+ 1	+ 1	+ 1	+ 1
I^{10}	+ 1	− 1	− 0	$\langle L_z \rangle$	0	$\langle L_z \rangle$	+ 1	− 1	− 0	+ 1	− 1	− 0
I^{20}	+ 1	+ 1	− 2	$\langle Q_{zz} \rangle$	0	$\langle Q_{zz} \rangle$	+ 1	+ 1	− 2	+ 1	+ 1	− 2
I^{01}				−	0	$\langle S_z \rangle$	+ 1	+ 1	+ 1	− 1	− 1	− 1
I^{11}				−	0	$\langle l \cdot s_z \rangle$	+ 1	− 1	− 0	− 1	+ 1	− 0
I^{21}				−	0	$\langle T_z \rangle$	+ 1	+ 1	− 2	− 1	− 1	+ 2

One can combine the spin sum rule with the circular dichroism sum rule. This implies circular dichroic excitation and spin-polarized detection of the valence (3d) electrons. According to the $\mathcal{T}^{11}$ spin–orbit sum rule:

$$\langle \sum l_z(i) s_z(i) \rangle = 2c_1 \int (\sigma_{L+} - \sigma_{R+}) - (\sigma_{L-} - \sigma_{R-}) \quad (10)$$

which is the sum of the spin–orbit interactions of the individual electrons. This sum rule can be viewed as a combination of the sum rules for $\langle L_z \rangle = \Sigma l_z(i)$ and $\langle S_z \rangle = \Sigma s_z(i)$. The combination of linear dichroism and spin-polarized detection gives the spin-quadrupole sum rule $\mathcal{T}^{21}$:

$$\langle \sum q_{zz}(i,j) s_z(i) \rangle = 2c_2 \int (2\sigma_{Z+} - \sigma_{L+} - \sigma_{R+}) - (2\sigma_{Z-} - \sigma_{L-} - \sigma_{R-}) \quad (11)$$

The spin-quadrupole operator can be compared with the magnetic dipole operator, indicated by the symbol $\langle _T z \rangle$. Apart from these six basic sum rules, additional sum rules have been developed. These sum rules use the fact that the 2p edges of the transition metal compounds are split into the L_3 and L_2 edges, separated by the 2p spin–orbit coupling, thereby continuing the work on the branching ratio (Eq. (4)). Two additional sum rules can be derived from a linear combination of the L_3 and L_2 edges. These sum rules do not measure a single moment, but instead a combination of them. The first of these effective sum rules determines a linear combination of the spin-moment and the magnetic dipole operator. This is because both moments couple to an effective spin-operator $\langle S_e \rangle$, which equals $\sum \langle s_z(i) \rangle + \frac{7}{2} \sum \langle t_z(i) \rangle$.

The effective-spin sum rule is:

$$\langle S_e \rangle = \tfrac{3}{2} \int_{L_3} (\sigma_L - \sigma_R) - 3 \int_{L_2} (\sigma_L - \sigma_R) \quad (12)$$

This sum rule implies some additional approximations. The sum rule is only correct if the L_3 and L_2 edges in the isotropic spectrum have a ratio of two to one (see the discussion of the branching ratio).

Table 1 indicates how to calculate the six fundamental spectra and what is obtained by integrating their spectral shapes. A distinction is made between 2p-XPS and 3d-XPS. All sum rules for core photoemission, such as 2p-XPS, are zero except for the overall signal. Note that both 2p-XAS and 3d-XPS determine the expectation values of the 3d-band. The 3d-band serves as electron source in 3d-XPS while in 2p-XAS the electron is excited into the 3d band (see also Section 5).

A detailed review on the X-ray absorption sum rules is given by Paolo Carra in this issue.

5. X-ray photoemission

The sum rule aspects of spin-polarized photoemission have been discussed in the previous section. This section discusses Theo's papers on the theory of photoemission spectra.

5.1. Fundamental theory

The fundamental theory of photoemission was discussed in the series of four papers 'Spin polarization and magnetic dichroism in photoemission from core

Table 2
Core p photoemission spectra and their sensitivity to the magnetic moments. The middle column indicates the values of X-ray polarization P, electron-spin P_s and magnetization M

Spectrum	$I(P,P_s,(M))$	Moment
Isotropic spectrum	$I^{00(0)}$	
Circular dichroism spectrum	$I^{10(1)}$	$\langle M\rangle$
Linear dichroism spectrum	$I^{20(2)}$	$\langle M^2\rangle$
Spin spectrum	$I^{01(1)}$	$\langle M\rangle$
Spin–orbit spectrum	$I^{11(0)}$	
Spin magnetic dipole spectrum	$I^{21(1)}$	$\langle M\rangle$
Spin–orbit quadrupole spectrum	$I^{11(2)}$	$\langle M^2\rangle$
Spin magnetic octupole spectrum	$I^{21(3)}$	$\langle M^3\rangle$

and valence states in localized magnetic systems'. Part I [42] introduces the eight fundamental spectra, Part II [64] discusses emission from open shells, Part III [74] the angular distribution, and Part IV [79] core hole polarization in resonant photoemission.

If the sum rules are applied to core photoemission the results are all zero because a core state has no moments. This does not imply that the spectral shapes are also zero everywhere. In fact, in Part I [42] it was shown that in the presence of electrostatic interactions between the created hole and magnetically polarized valence electrons, one can distinguish eight fundamental spectra. These eight spectra are given in Table 2. They relate to the six sum rules as given in the previous section: the I^{00} isotropic spectrum, the I^{10} circular dichroism spectrum, the I^{20} linear dichroism spectrum, the I^{01} spin spectrum, the I^{11} spin–orbit spectrum and the I^{21} spin magnetic dipole spectrum. The two last combinations of circular respectively linear dichroism plus spin-detection couple to a second magnetic moment expectation value. One can distinguish between $I^{11(0)}$ and $I^{11(2)}$ for the spin–orbit and between $I^{21(1)}$ and $I^{21(3)}$ for the spin magnetic dipole spectrum (see [42,64]).

In Part II, 'Emission from open shells' [64], it was shown that for emission from an incompletely filled shell the integrated intensities of the fundamental spectra are proportional to the expectation values of the number of electrons, spin magnetic moment, orbital magnetic moment, the alignment between orbital and spin magnetic moment, the quadrupole moment, and the correlation between quadrupole and spin magnetic moment, respectively.

The situations for valence excitations and core

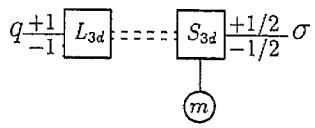

Fig. 8. Photoemission process with X-ray polarization $q = \pm 1$ and electron spin $\sigma = \pm 1/2$ acting directly on the 3d valence band.

excitations is sketched in the following three figures: the photoemission from a 3d valence shell is indicated in Fig. 8 (based on Fig. 1 in [42]). Spin-polarized detection of the 3d photoemission determines directly the spin-moment $\langle S_{3d}\rangle$, i.e. the magnetic moment m. Circular dichroic excitation is sensitive to the orbital moment $\langle L_{3d}\rangle$, which couples by spin–orbit coupling to the spin-moment.

Fig. 9 sketches the situation for 2p photoemission, as described within a relativistic single-particle picture. Spin-polarized detection of the 2p-photoemission acts on the 2p spin-moment, which is coupled by exchange to the 3d spin-moment. This creates a spin-polarized 2p photoemission spectrum. Circular dichroic excitation is sensitive to the orbital moment $\langle L_{2p}\rangle$, which is coupled by the strong core spin–orbit coupling to the 2p spin-moment. Together with the 2p3d exchange this creates an MCD spectral shape for 2p photoemission.

Describing the same process of 2p photoemission with a multiplet picture adds an interaction between the orbital moments as indicated in Fig. 10. In the case of 3d transition metals, rare earths and actinides, this interaction is very strong and completely changes the spectral shape of the MCD spectra. Fig. 11 shows the 3p spin-polarized photoemission spectra of Cu^{2+}. The calculations are carried out for transitions from $3d^9 + 3d^{10}\underline{L} \rightarrow 3p^5 3d^9 \varepsilon_d + 3p^5 3d^{10}\underline{L}\varepsilon_d$. More examples are given in [42,64].

In Part III, 'Angular distribution' [74], a general

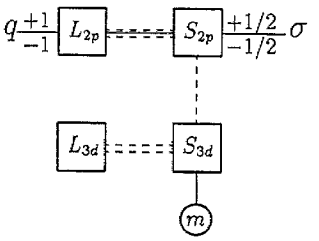

Fig. 9. Single-particle picture of the photoemission process with X-ray polarization $q = \pm 1$ and electron spin $\sigma = \pm 1/2$ acting on the 2p core states.

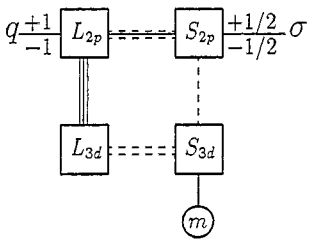

Fig. 10. Multiplet picture of the photoemission process with X-ray polarization $q = \pm 1$ and electron spin $\sigma = \pm 1/2$ acting on the 2p core states.

analysis was presented for angle-dependent photoemission from magnetic and oriented atoms using linearly and circularly polarized X-rays. The anisotropy in the angular distribution (ε) is determined by the polarization of the photon (P) and the magnetic moments of the system (M). For localized (strongly correlated) systems the magnetic moment affects the polarization of the shell from which the electron is emitted (e.g. 2p), via the spin–orbit couplings and the Coulomb and exchange interactions of the hole with the polarized valence electrons in the final state of the photoionized atom (see Fig. 10).

In [74,75], the angular dependence is indicated with the function $U^{abx}(M,\varepsilon,P)$. From the analysis, it follows that linear dichroism measured in angular-distribution (LDAD) is sensitive to the magnetic moment $\langle M\rangle$,

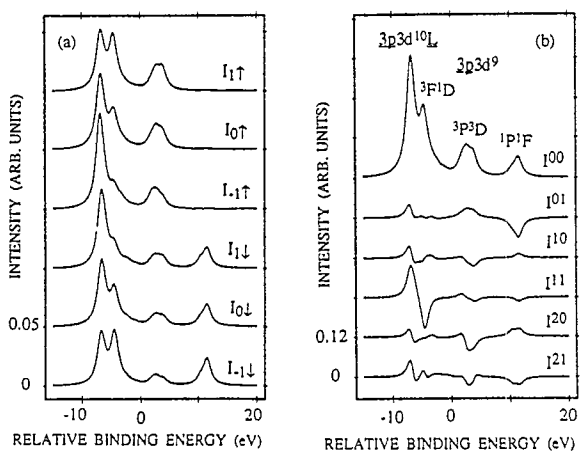

Fig. 11. Charge transfer multiplet calculations for Cu 3p spin-polarized photoemission. On the left the six primitive spectra and on the right the six fundamental spectra are shown. (Reproduced with permission from Ref. [42]. Copyright 1991 American Physical Society.)

Table 3
Comparision of CD and LD with their angle-distributed analogues CDAD and LDAD. The values for b in the angular functions U are even. They are respectively U^{101} and U^{121} for CD and U^{202}, U^{222} and U^{242} for LD

Spectrum	$I(P)$	$U(M,\varepsilon,P)$	Moment
CD	I^1	U^{1b1}	$\langle M\rangle$
CDAD	I^1	U^{221}	$\langle M^2\rangle$
LD	I^2	U^{2b2}	$\langle M^2\rangle$
LDAD	I^2	U^{122}	$\langle M\rangle$

while CDAD is sensitive to the squared moment $\langle M^2\rangle$, as indicated in Table 3. Thus, one is sensitive to the magnetic moment $\langle M\rangle$ with CD and with LDAD. This implies that one has the choice of using circular polarized X-rays and studying CD or using linear polarized X-rays and studying the angular dependence of the emitted electrons.

In Part IV, 'Core hole polarization in resonant photoemission' [79,80], a theory was presented for core hole polarization probed by spin polarization (P_S) and magnetic dichroism (P) in resonant photoemission. The resonant photoemission is considered as a two-step process, starting with an excitation from a core level to the valence shell, after which the core hole decays into two shallower core holes while an electron is emitted. The two core holes form well-defined states which can be selected by the energy of the emitted electron. The intensity is a sum over ground state expectation values of tensor operators $W(P,P_S,M)$ multiplied by the probability of creating a polarized core hole using polarized light $U(M,P,P_S,\varepsilon)$, multiplied by the probability for decay of such a core hole $\boldsymbol{B}$. It is shown that the calculation of the spectral shapes can be separated into these three parts:

$$J(M,P,P_S,\varepsilon)=\boldsymbol{W}\cdot\boldsymbol{U}\cdot\boldsymbol{B}$$

This core polarization analysis generalizes the use of sum rules in X-ray absorption spectroscopy where the integrated peak intensities give ground state expectation values of operators such as the spin and orbital moments. The photoemission decay makes it possible to measure new linear combinations of operators. The general formula for second-order processes shows that in the presence of core–valence interactions the two-step model may break down due to interference terms between intermediate states separated by more

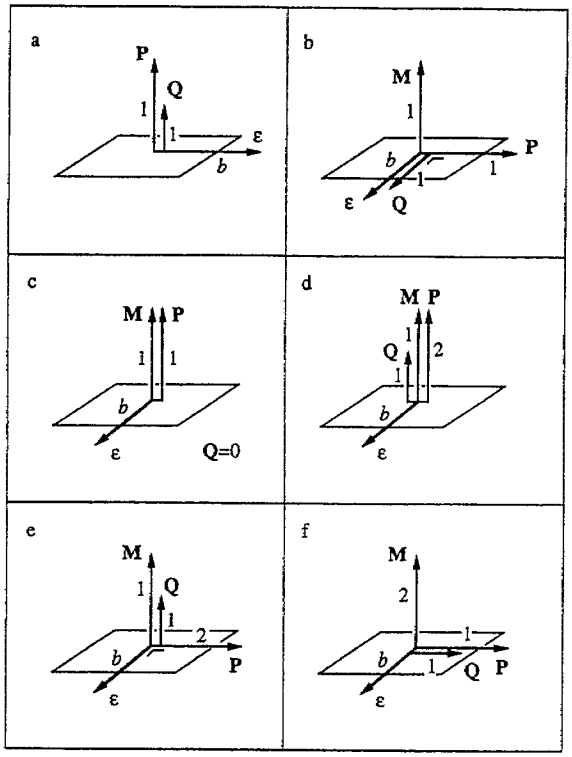

Fig. 12. Geometries in which the direction of Q is fixed by the general properties of the angle-dependent functions: (a) $M^0 \Rightarrow Q \| P$; (b) $\varepsilon \perp P \perp M \Rightarrow Q \| \varepsilon$; (c) $\varepsilon \perp P \| M \Rightarrow Q = 0$; (d) $\varepsilon \perp P^2 \| M \Rightarrow Q \| M$; (e) $\varepsilon \perp P^2 \perp M \Rightarrow Q \| M$; (f) $M^2 \Rightarrow Q \| P$. (Reproduced with permission from Ref. [79]. Copyright 1995 American Physical Society.)

than their lifetime width. This situation is analogous to the interference effects in resonant X-ray scattering (see Section 6).

Fig. 12 sketches the consequences for a series of angular combinations of the X-ray polarization P, the electron direction ε and its polarization Q (i.e. the polarization vector of P_S) and the magnetic moment M. The figure shows the possibilities for the direction of Q, depending on the relative directions of P, M and ε. For a discussion of these rules see [74].

In 'Core hole polarization in X-ray absorption studied by magnetic circular dichroism in 2p3p3p resonant photoemission' [78] it was shown that the possibilities of X-ray absorption can be strongly increased when the polarization of the core hole is detected by the angle dependence of the resonant photoemission. In the geometry where the dichroism in the 2p absorption is forbidden, a large circular dichroism is observed in the autoionization decay into a $3p^4$ state.

5.2. Photoemission of the rare earths

In 'La 5p core photoemission spectra at the 4d4f resonance in LaF_3' [61] an anomalous change of the photoemission branching ratio between $5p_{1/2}$ and $5p_{3/2}$ intensities at $^3P_1$ and $^3D_1$ resonances is observed by energy distribution curves and constant-initial-state spectra. This change of the branching ratio was attributed to the multiplet dependence of the Auger transition probabilities. In 'Lifetime effect on the multiplet structure of 3d X-ray photoemission spectra in heavy rare-earth elements' [77] it was shown that the lifetime broadening of the states in the multiplets strongly varies with their binding energies. The generally adopted assumption of the constant core hole lifetime broadening breaks down completely if the coupling between a core hole and unfilled valence shell is strong and yet the decay process is dominated by the coupling between them.

In 'Multiplet fine structure in the photoemission of the gadolinium and terbium 5p levels' [63] it was shown that calculated theoretical spectra are in good agreement with experimental results.

5.3. Photoemission of nickel

The 'Electronic correlations in Ni 2p and 3p magnetic X-ray dichroism and X-ray photoemission of nickel' [53] were analyzed using an Anderson impurity model taking into account multiplet splitting. Good agreement with the experimental result has been obtained for a ground state of 18% d^8, 49% d^9 and 33% d^{10} character. 'Strong resonances in core-level photoemission' [54] were predicted with a deeper core-level absorption. This allows a straightforward interpretation of core level spectroscopy in two ways: (a) photoemission peaks can be resolved in resonance with different X-ray absorption peaks, and (b) X-ray absorption peaks can be resolved using partial electron yield at constant binding energy. In 'Resonant photoemission at the Ni 2p core level as a probe of electron correlation effects in nickel' [55] the observed enhancement in the 3d, 3p and 3s photoemission structures was analyzed using a cluster calculation including multiplet structure. The result

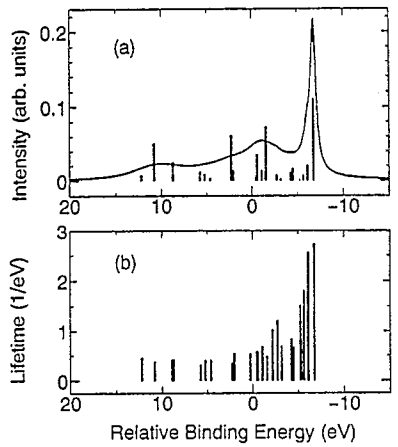

Fig. 13. Theoretical nickel 3p photoemission (top) and the lifetime of each multiplet state (bottom). (Reproduced with permission from Ref. [70]. Copyright 1993 American Physical Society.)

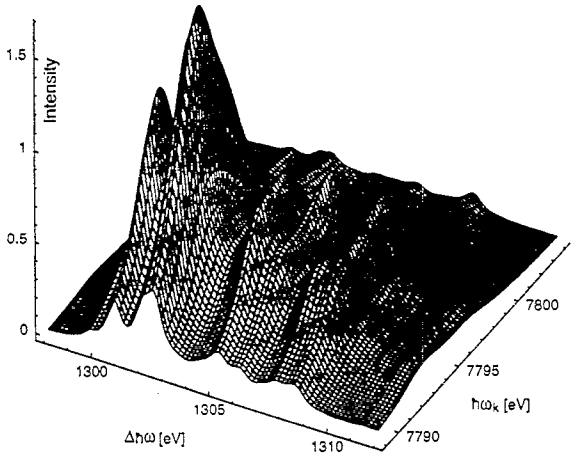

Fig. 14. Calculation of the transition $4f^{10} \rightarrow 2p^5 4f^{11} \rightarrow 3d^9 4f^{11}$ at the Dy L_3 edge as a function of ω and $\Delta\omega = \omega - \omega'$. (Reproduced with permission from Ref. [83]. Copyright 1995 American Physical Society.)

strongly supports the view of a localized electronic structure for nickel metal. The Ni 3p photoemission of ferromagnetic nickel shows a magnetic circular dichroism which is much larger than expected from the value of the bulk orbital moment. In 'Surface orbital magnetic moment of nickel studied by MCD in Ni 3p photoemission' [56] it was argued that the strong magnetic dichroism in photoemission can only be explained when the orbital moment at the surface is strongly enhanced as predicted recently by band structure calculations.

In 'Auger decay of quasiparticle states: calculation of the Ni 3p photoemission spectrum in $NiCl_2$' [70] it was shown that the LS-term dependence of the lifetimes strongly affects the whole spectral shape because the multiplet splitting of the 3p-XPS is large. Fig. 13 (reproduced from [70]) shows that the lifetime broadening increases from about 0.5 eV to about 2.5 eV over the 3p-XPS spectral range. Because the 2p core state has a much stronger spin–orbit coupling, the LS-terms are mixed and a less strong state dependence of the lifetime broadening occurs.

6. Resonant X-ray scattering

High-resolution X-ray resonant Raman scattering [83] gives a general formulation of X-ray resonant Raman scattering. The scattering of X-rays from a ground state (energy E_0), via an intermediate state (energy E_x, lifetime broadening Γ_x) to a final state (energy E_f, lifetime broadening Γ_f) is given as:

$$I_{(\hbar\omega,\hbar\omega')} = \sum_{qq'} \sum_{f} \left| \sum_{x} \frac{<f|r_q'|x> <x|r_q|i_0>}{E_0 + \hbar\omega - E_x - i\Gamma_x} \right|^2 \times \delta_{(E_f + \hbar\omega' - E_0 - \hbar\omega)} \quad (13)$$

The incoming X-ray has energy $\hbar\omega$ and the emitted X-ray has energy $\hbar\omega'$. Below all factors of $\hbar$ are omitted. Assuming a single intermediate state, it can be derived from Eq. (13) that a spectrum at fixed emission energy ω', indicated as $I(\omega)|_{\omega'}$, has a lifetime broadening equal to Γ_x. A spectrum scanning the final state, i.e. $I(\omega' - \omega)|_{\omega}$, has a lifetime broadening Γ_f. The "resonant X-ray emission spectrum" $I(\omega')|_{\omega}$ relates to a 45° cross-section in Fig. 14. Its lifetime broadening is neither Γ_x nor Γ_f. Note that for a single intermediate state, the lifetime broadening is equal to: $\Gamma_{RXES} = 1/\left(\frac{1}{\Gamma_x} + \frac{1}{\Gamma_f}\right)$, which is less than both Γ_x and Γ_f. Often $\Gamma_x \gg \Gamma_f$ and $\Gamma_{RXES} \approx \Gamma_f$.

In [83] it is shown that the presence of more than one intermediate state and the inclusion of many-body effects drastically alter the interpretation of the resonances. Fig. 14 shows the resonant Raman spectrum of dysprosium at the $2p_{3/2} \rightarrow 4f$ quadrupole excitation (at about 7790 eV) for its $3d_{5/2} \rightarrow 2p_{3/2}$ dipole decay (at about 1300 eV energy difference).

In 'Magnetic X-ray Compton scattering' [86] it was shown that the cross-section is found to be insensitive

to orbital effects, in agreement with recent experiments on transition metal and rare earth ferromagnets. When the transferred energy is sufficiently small to generate substantial corrections to the impulse approximation, the sensitivity to orbital moments of ordinary non-resonant magnetic scattering is recovered.

In 'Anisotropic X-ray anomalous diffraction and forbidden reflections' [76,82] a general analysis of resonant elastic scattering of X-rays is presented. The consequences of crystal symmetry, scattering geometry and polarization are outlined. Extinction rules, their breaking, and the observation of forbidden reflections are discussed. As an application, a detailed description of the experiment performed by Finkelstein, Shen and Shastri at the iron K edge in α-Fe_2O_3 is reported.

Acknowledgements

We thank the journal *Physical Review* and the authors Jeroen Goedkoop, Kozo Okada and Paolo Carra, for permission to reproduce their figures.

References

[1] B.T. Thole, P.T. van Duijnen, On the quantum-mechanical treatment of solvent effects, Theor. Chim. Acta 55 (1979) 307.

[2] S. Huizinga, J. Kommandeur, G.A. Sawatzky, B.T. Thole, K. Kopinga, W.J.M. de Jonge, J. Roos, Spin Peierls transition in MEM(TCNQ)$_2$, Phys. Rev. B 19 (1979) 4723.

[3] P.T. van Duijnen, B.T. Thole, W.G.J. Hol, On the role of the active site helix in papain, an ab initio molecular-orbital study, Biophys. Chem. 9 (1979) 273.

[4] P.T. van Duijnen, B.T. Thole, R. Broer, W.C. Nieuwpoort, Active site α-helix in papain and the stability of the ion pair RS–ImH$^+$, Int. J. Quantum Chem. 17 (1980) 651.

[5] B.T. Thole, Molecular polarizabilities calculated with a modified dipole interaction, Chem. Phys. 59 (1981) 341.

[6] P.T. van Duijnen, B.T. Thole, The α-helix as an ion channel. An ab initio molecular orbital study, Chem. Phys. Lett. 83 (1981) 129.

[7] B.T. Thole, P.T. van Duijnen, The direct reaction field hamiltonian: analysis of the dispersion term and application to the water dimer, Chem. Phys. 71 (1982) 211.

[8] P.T. van Duijnen, B.T. Thole, Cooperative effects in α-helices: an ab initio molecular orbital study, Biopolymers 21 (1982) 1749.

[9] P.T. van Duijnen, B.T. Thole, Electric fields of α-helices, Stud. Phys. Theor. Chem. 18 (1982) 347.

[10] B.T. Thole, P.T. van Duijnen, A general population analysis preserving the dipole moment, Theor. Chim. Acta 61 (1983) 209.

[11] B.T. Thole, P.T. van Duijnen, Reaction field effects on proton transfer in the active site of actinidin, Biophys. Chem. 18 (1983) 53.

[12] B.T. Thole, P.T. van Duijnen, J.C. de Jager, Ab initio calculations with the direct reaction field hamiltonian, in: Structure and Dynamics: Nucleic Acids and Proteins, Adenine Press, New York, 1983, p. 9.

[13] B.T. Thole, Least squares numerical Rayleigh–Ritz and minimum variance methods for molecular calculations, Int. J. Quantum Chem. 28 (1985) 535.

[14] P.T. van Duijnen, J.C. de Jager, B.T. Thole, Do parallel beta-strands have dipole moments: an ab initio molecular orbital direct reaction field study, Biopolymers 24 (1985) 735.

[15] B.T. Thole, R.D. Cowan, G.A. Sawatzky, J. Fink, J.C. Fuggle, New probe for the ground state electronic structure of narrow band and impurity states, Phys. Rev. B 31 (1985) 6856.

[16] B.T. Thole, G. van der Laan, G.A. Sawatzky, Strong magnetic dichroism predicted in the $M_{4,5}$ X-ray absorption spectra of magnetic rare earth materials, Phys. Rev. Lett. 55 (1985) 2086.

[17] B.T. Thole, G. van der Laan, J.C. Fuggle, G.A. Sawatzky, R.C. Karnatek, J.M. Esteva, 3d X-ray absorption lines and the $3d^94f^{n+1}$ multiplets of the lanthanides, Phys. Rev. B 32 (1985) 5107.

[18] G. van der Laan, B.T. Thole, G.A. Sawatzky, J.B. Goedkoop, J.C. Fuggle, J.-M. Esteva, R. Karnatak, J.P. Remeika, H.A. Dabkowska, Experimental proof of magnetic X-ray dichroism, Phys. Rev. B 34 (1986) 6529.

[19] G. van der Laan, B.T. Thole, J. Zaanen, G.A. Sawatzky, J.C. Fuggle, R.C. Karnatak, J.M. Esteva, Multiplet effects in near edge XAS for ground state studies, J. Phys. (Paris) Colloq. C 8 (1986) 997.

[20] G. van der Laan, B.T. Thole, G.A. Sawatzky, J.C. Fuggle, R.C. Karnatak, J.M. Esteva, B. Lengeler, Identification of the relative population of spin–orbit split states in the ground state of a solid, J. Phys. C 19 (1986) 817.

[21] B.T. Thole, G. van der Laan, Systematics of the relation between spin–orbit splitting in the valence band and the branching ratio in X-ray absorption spectra, Europhys. Lett. 4 (1987) 1083.

[22] L. Degiorgi, T. Greber, F. Hulliger, R. Monnier, L. Schlapbach, B.T. Thole, 3d core level photoemission spectra of heavy lanthanides: YbP, Europhys. Lett. 4 (1987) 755.

[23] B.T. Thole, G. van der Laan, P.H. Butler, Spin-mixed ground state of Fe phthalocyanine and the temperature-dependent branching ratio in X-ray absorption spectroscopy, Chem. Phys. Lett. 149 (1988) 295.

[24] B.T. Thole, G. van der Laan, Branching ratio in X-ray absorption spectroscopy, Phys. Rev. B 38 (1988) 3158.

[25] B.T. Thole, G. van der Laan, Linear relation between X-ray absorption branching ratio and valence-band spin–orbit expectation value, Phys. Rev. A 38 (1988) 1943.

[26] G. van der Laan, B.T. Thole, Determination of glitches in soft X-ray monochromator crystals, Nucl. Instrum. Methods A 263 (1988) 515.

[27] G. van der Laan, B.T. Thole, Angular dependent photoelectric yield. Measurement of the La3d Auger and autoionization lifetime widths, J. Electron Spectrosc. Relat Phenom. 46 (1988) 123.
[28] G. van der Laan, B.T. Thole, Local probe for spin–orbit interaction, Phys. Rev. Lett. 60 (1988) 1977.
[29] G. van der Laan, B.T. Thole, G.A. Sawatzky, M. Verdaguer, Multiplet structure in the $L_{2,3}$ X-ray absorption spectra: a fingerprint for high- and low-spin Ni^{2+} and Cu^{3+} compounds, Phys. Rev. B 37 (1988) 6587.
[30] J.B. Goedkoop, B.T. Thole, G. van der Laan, G.A. Sawatzky, F.M.F. de Groot, J.C. Fuggle, Calculations of magnetic X-ray dichroism in the 3d absorption spectra of the rare earths, Phys. Rev. B 37 (1988) 2086.
[31] J.B. Goedkoop, J.C. Fuggle, B.T. Thole, G. van der Laan, G.A. Sawatzky, Circularly polarized line filters in the soft X-ray range, Nucl. Instrum. Methods A 273 (1988) 429.
[32] J.B. Goedkoop, J.C. Fuggle, B.T. Thole, G. van der Laan, G.A. Sawatzky, Magnetic X-ray dichroism of rare earth materials, J. Appl. Phys. 64 (1988) 5595.
[33] F.U. Hillebrecht, V. Sechovsky, B.T. Thole, Dilute uranium alloys: test cases for the 5f electronic structure, J. Magn. Magn. Mater. 76–77 (1988) 353.
[34] F.U. Hillebrecht, H.J. Trodahl, V. Sechovsky, B.T. Thole, U impurities in Au, Z. Phys. B 77 (1989) 373.
[35] A. Kotani, H. Ogasawara, K. Okada, B.T. Thole, G.A. Sawatzky, Theory of multiplet structure in 4d core photoabsorption spectra of CeO_2, Phys. Rev. B 40 (1989) 65.
[36] G. van der Laan, B.T. Thole, Magnetic dichroism in the X-ray absorption branching ratio, Phys. Rev. B 42 (1990) 6670.
[37] F.M.F. de Groot, J.C. Fuggle, B.T. Thole, G.A. Sawatzky, $L_{2,3}$ X-ray absorption edges of d_0 compounds: K^+, Ca^{2+}, Sc^{3+} and Ti^{4+} in O_h (octahedral symmetry), Phys. Rev. B 41 (1990) 928.
[38] F.M.F. de Groot, J.C. Fuggle, B.T. Thole, G.A. Sawatzky, 2p X-ray absorption of 3d transition-metal compounds: an atomic multiplet description including the crystal field, Phys. Rev. B 42 (1990) 5459.
[39] F.M.F. de Groot, M. Grioni, J.C. Fuggle, B.T. Thole, J. Ghijsen, G.A. Sawatzky, Ligand field effects in XAS of 3d transition metal compounds, Proc. XSRR, Eds. A. Balerna, E. Bernieri and S. Mobilio, SIF, Bologna, 1990.
[40] A.B. van Oosten, R. Broer, B.T. Thole, W.C. Nieuwpoort, Cluster calculation on localized holes in La_2CuO_4, J. Less-Common Metals 164 (1990) 1514.
[41] K. Okada, A. Kotani, B.T. Thole, G.A. Sawatzky, Polarization dependence of core-level XPS in anisotropic solids, Solid State Commun. 76 (1990) 1277.
[42] B.T. Thole, G. van der Laan, Spin polarization and magnetic dichroism in photoemission from core and valence states in localized magnetic systems, Phys. Rev. B 44 (1991) 12424.
[43] B.T. Thole, G. van der Laan, Origin of spin polarization and magnetic dichroism in core level photoemission, Phys. Rev. Lett. 67 (1991) 3306.
[44] G. van der Laan, B.T. Thole, Strong magnetic X-ray dichroism in 2p absorption spectra of 3d transition-metal ions, Phys. Rev. B 43 (1991) 13401.
[45] M. Abbate, F.M.F. de Groot, J.C. Fuggle, A. Fujimori, Y. Tokura, Y. Fujishima, O. Strebel, M. Domke, G. Kaindl, J. van Elp, B.T. Thole, G.A. Sawatzky, M. Sacchi, N. Tsuda, Soft X-ray absorption studies of the electronic structure of controlled-valence materials, Phys. Rev. B 44 (1991) 5419.
[46] P. Carra, B.N. Harmon, B.T. Thole, M. Altarelli, G.A. Sawatzky, Magnetic X-ray dichroism in gadolinium metal, Phys. Rev. Lett. 66 (1991) 2495.
[47] H. Ogasawara, A. Kotani, R. Potze, G.A. Sawatzky, B.T. Thole, Praseodymium 3d and 4d core photoemission spectra of Pr_2O_3, Phys. Rev. B 44 (1991) 5465.
[48] H. Ogasawara, A. Kotani, K. Okada, B.T. Thole, Theory of X-ray absorption spectra in PrO_2 and some other rare earth compounds, Phys. Rev. B 43 (1991) 854.
[49] H. Ogasawara, A. Kotani, B.T. Thole, Calculation of magnetic X-ray dichroism in 4d and 5d absorption spectra of actinides, Phys. Rev. B 44 (1991) 2169.
[50] F.J. Himpsel, U.O. Karlsson, A.B. McLean, L.J. Terminello, F.M.F. de Groot, M. Abbate, J.C. Fuggle, J.A. Yarmoff, B.T. Thole, G.A. Sawatzky, Fine structure of the Ca 2p X-ray absorption edge for bulk compounds, surfaces and interfaces, Phys. Rev. B 43 (1991) 6899.
[51] K. Okada, A. Kotani, B.T. Thole, G.A. Sawatzky, Evidence of local singlet state in $NaCuO_2$ from Cu 2p X-ray photoemission and photoabsorption spectra, Solid State Commun. 77 (1991) 835.
[52] B.T. Thole, P. Carra, F. Sette, G. van der Laan, X-ray circular dichroism as a probe of orbital magnetization, Phys. Rev. Lett. 68 (1992) 1943.
[53] G. van der Laan, B.T. Thole, Electronic correlations in Ni 2p and 3p magnetic X-ray dichroism and X-ray photoemission of ferromagnetic nickel, J. Phys.: Condens. Matter 4 (1992) 4181.
[54] G. van der Laan, B.T. Thole, H. Ogasawara, Y. Seino, A. Kotani, Strong resonances in core-level photoemission, Phys. Rev. B 46 (1992) 7221.
[55] G. van der Laan, M. Surman, M.A. Hoyland, C.F.J. Flipse, B.T. Thole, Y. Seino, H. Ogasawara, A. Kotani, Resonant photoemission at the Ni 2p core level as a probe of electron correlation effects in nickel, Phys. Rev. B 46 (1992) 9336.
[56] G. van der Laan, B.T. Thole, Classification for angle dependent polarized photoemission spectra using magnetic moment analysis, Solid State Commun. 92 (1994) 427 .
[57] M. Abbate, F.M.F. de Groot, J.C. Fuggle, A. Fujimori, O. Strebel, F. Lopez, M. Domke, G. Kaindl, B.T. Thole, G.A. Sawatzky, M. Takano, Y. Takeda, H. Eisaki, S. Uchida, Controlled-valence properties of $La_{1-x}Sr_xFeO_3$ and $La_{1-x}Sr_xMnO_3$ studied by soft X-ray absorption spectroscopy, Phys. Rev. B 46 (1992) 4511.
[58] K. Okada, A. Kotani, B.T. Thole, Charge transfer satellites and multiplet splitting in X-ray photoemission spectra of late transition metal halides, J. Electron Spectrosc. Relat. Phenom. 58 (1992) 325.
[59] Y. Seino, H. Ogasawara, A. Kotani, B.T. Thole, G. van der Laan, Calculation of Cu 2p resonant photoemission spectra in CuO, J. Phys. Soc. Jpn. 61 (1992) 1859.
[60] C.C. Tang, W.G. Stirling, G.H. Lander, D. Gibbs, W. Herzog,

P. Carra, B.T. Thole, K. Mattenberger, O. Vogt, Resonant magnetic X-ray scattering in a series of uranium compounds, Phys. Rev. B 46 (1992) 5287.

[61] H. Ogasawara, A. Kotani, B.T. Thole, K. Ichikawa, O. Aita, M. Kamada, La 5p core photoemission spectra at the 4d4f resonance in LaF_3, Solid State Commun. 81 (1992) 645.

[62] B.T. Thole, G. van der Laan, Sum rules for magnetic dichroism in rare earth 4f photoemission, Phys. Rev. Lett. 70 (1993) 2499.

[63] B.T. Thole, X.D. Wang, B.N. Harmon, Dongqi Li, P.A. Dowben, Multiplet fine structure in the photoemission of the gadolinium and terbium 5p levels, Phys. Rev. B 47 (1993) 9098.

[64] G. van der Laan, B.T. Thole, Spin polarization and magnetic dichroism in photoemission from core and valence states in localized magnetic systems. II. Emission from open shells, Phys. Rev. B 48 (1993) 210.

[65] P. Carra, B.T. Thole, M. Altarelli, X. Wang, X-ray circular dichroism and local magnetic fields, Phys. Rev. Lett. 70 (1993) 694.

[66] P. Carra, H. König, B.T. Thole, M. Altarelli, Magnetic X-ray dichroism. General features of dipolar and quadrupolar spectra, Physica B 192 (1993) 182.

[67] L.H. Tjeng, C.T. Chen, P. Rudolf, G. Meigs, G. van der Laan, B.T. Thole, Magnetic circularly polarized 2p resonant photoemission of nickel, Phys. Rev. B 48 (1993) 13378.

[68] C.J.F. Flipse, G. van der Laan, B.T. Thole, S. Myhra, Polarized X-ray absorption study of $Bi_2Sr_2CuO_6$ and Bi_2Sr_2. $CaCu_2uO_8$, Z. Phys. B 90 (1993) 89.

[69] D.B. McWhan, E.D. Isaacs, Paolo Carra, S.M. Shapiro, B.T. Thole, S. Hoshino, Resonant magnetic X-ray scattering from mixed-valence TmSe, Phys. Rev. B 47 (1993) 8630.

[70] K. Okada, A. Kotani, H. Ogasawara, Y. Seino, B.T. Thole, Auger decay of quasiparticle states: calculation of the Ni 3p photoemission spectrum in $NiCl_2$, Phys. Rev. B 47 (1993) 6203.

[71] B.T. Thole, Information in polarized X-ray absorption spectroscopy and photoemission spectroscopy, J. Appl. Phys. 10 (1994) 5807.

[72] B.T. Thole, G. van der Laan, M. Fabrizio, Magnetic ground-state properties and spectral distributions. I. X-ray absorption spectra, Phys. Rev. B 50 (1994) 11466.

[73] B.T. Thole, G. van der Laan, Magnetic ground-state properties and spectral distributions. II. Polarized photoemission, Phys. Rev. B 50 (1994) 11474.

[74] B.T. Thole, G. van der Laan, Spin polarization and magnetic dichroism in photoemission from core and valence states in localized magnetic systems. III. Angular distribution, Phys. Rev. B 49 (1994) 9613.

[75] G. van der Laan, M.A. Hoyland, M. Surman, C.F.J. Flipse, B.T. Thole, Surface orbital magnetic moment of ferromagnetic nickel studied by circular magnetic dichroism in Ni 3p core level photoemission, Phys. Rev. Lett. 69 (1992) 3827; Erratum, 70 (1993) 1186.

[76] P. Carra, B.T. Thole, Anisotropic X-ray anomalous diffraction and forbidden reflections, Rev. Mod. Phys. 66 (1994) 1509.

[77] H. Ogasawara, A. Kotani, B.T. Thole, Lifetime effect on the multiplet structure of 3d X-ray photoemission spectra in heavy rare-earth elements, Phys. Rev. B 50 (1994) 12332 .

[78] B.T. Thole, H.A. Dürr, G. Van der Laan, Core hole polarization in X-ray absorption studied by magnetic circular dichroism in 2p3p3p resonant photoemission, Phys. Rev. Lett. 74 (1995) 2371.

[79] G. van der Laan, B.T. Thole, Spin polarization and magnetic dichroism in photoemission from core and valence states in localized magnetic systems. IV. Core hole polarization in resonant photoemission, Phys. Rev. B 52 (1995) 15355.

[80] G. van der Laan, B.T. Thole, Core hole polarization in resonant photoemission, J. Phys.: Condens. Matter 7 (1995) 9947.

[81] D. Alders, J. Vogel, C. Levelut, S.D. Peacor, T. Hibma, M. Sacchi, L.H. Tjeng, C.T. Chen, G. van der Laan, B.T. Thole, G.A. Sawatzky, Magnetic X-ray dichroism study of the nearest neighbour spin–spin correlation function and long range magnetic order parameter in antiferromagnetic NiO, Europhys. Lett. 32 (1995) 259.

[82] P. Carra, B.T. Thole, Anisotropic X-ray anomalous diffraction and forbidden reflections in Fe_2O_3, Vacuum 46 (1995) 1105.

[83] P. Carra, M. Fabrizio, B.T. Thole, High resolution X-ray resonant Raman scattering, Phys. Rev. Lett. 74 (1995) 3700.

[84] A.H. de Vries, P.Th. van Dijnen, J.A.C. Rullman, J.P. Dijkman, H. Merenga, B.T. Thole, Implementation of reaction field methods in quantum chemistry computer codes, J. Comput. Chem. 16 (1995) 37.

[85] G. van der Laan, B.T. Thole, X-ray absorption sum rules in *jj*-coupled operators and ground state moments of actinide ions, Phys. Rev. B 53 (1996) 14458.

[86] P. Carra, M. Fabrizio, G. Santoro, B.T. Thole, Magnetic X-ray Compton scattering, Phys. Rev. B 53 (1996) 5994.

[87] J.P. Crocombette, B.T. Thole, F. Jollet, The importance of the magnetic dipole term in MCD for 3d transition metal compounds, J. Phys.: Condens. Matter 8 (1996) 4095.

[88] H.A. Dürr, G.Y. Guo, B.T. Thole, G. van der Laan, Magnetocrystalline anisotropy of ultrathin Fe films in Ni(110), J. Phys.: Condens. Matter, 8 (1996) 111.

[89] H.A. Dürr, G. van der Laan, B.T. Thole, Microscopic origin of magnetocrystalline anisotropy in Au/Co/Au probed with X-MCD (comment), Phys. Rev. Lett. 76 (1996) 3464.

[90] Y. Teramura, A. Tanaka, B.T. Thole and T. Jo, Effect of Coulomb interaction on the X-ray MCD spin sum rule, J. Phys. Soc. Jpn. 65 (1996) 3056.

[91] T. Fujii, D. Alders, F.C. Voogt, T. Hibma, B.T. Thole, G.A. Sawatzky, In situ RHEED and XPS studies of epitaxial thin α-Fe_2O_3(0001) films on sapphire, Surf. Sci. 366 (1996) 579.

[92] M. van Veenendaal, J.B. Goedkoop, B.T. Thole, Branching ratios of the circular dichroism at rare earth $L_{2,3}$ edges, J. Electron Spectrosc. Relat. Phenom. 86 (1997) 151.

[93] J.B. Goedkoop, N. Brookes, M. van Veenendaal, B.T. Thole, Soft X-ray fluorescence yield X-ray MCD sum rules, J. Electron Spectrosc. Relat. Phenom. 86 (1997) 143.

[94] G. van der Laan, B.T. Thole, Anisotropic branching ratio in X-ray absorption spectra, J. Electron Spectrosc. Relat. Phenom. 86 (1997) 57.